

## Micromachined Silicon Cantilever Paddle for High-Flow-Rate Sensing

Rong-Hua Ma, Ming-Chin Ho<sup>1</sup>, Chia-Yen Lee<sup>2,\*</sup>, Yu-Hsiang Wang<sup>2</sup>  
and Lung-Ming Fu<sup>3</sup>

Department of Mechanical Engineering, Chinese Military Academy, Kaohsiung, Taiwan 830

<sup>1</sup>Architecture and Building Research Institute, Ministry of the Interior, Taipei Taiwan 231

<sup>2</sup>Department of Mechanical and Automation Engineering, Da-Yeh University,  
Chung-hua, Taiwan 515

<sup>3</sup>Graduate Institute of Materials Engineering,  
National Pingtung University of Science and Technology, Pingtung, Taiwan 912

(Received June 27, 2006; accepted November 14, 2006)

**Key words:** flow sensor, microcantilever, micro-electro-mechanical system (MEMS), residual stress

In this study, we exploit the bending-up of a cantilever paddle caused by residual stress to manufacture a micro-gas-flow-sensor for high-flow-rate sensing. Microsensors not only have a smaller physical size than their traditional counterparts, but also provide greater measurement accuracy and a higher sensitivity in the high gas flow velocity range. In this study, micro-electro-mechanical system (MEMS) techniques are used to deposit a silicon nitride layer on a silicon wafer to create a cantilever structure. A platinum layer is deposited on the silicon nitride layer to form a resistor and the structure is then etched to form a freestanding microcantilever. It is found that the cantilever slightly bends upward as a result of the released residual stress induced in the beam during the fabrication process. When airflow passes over the cantilever beam, a small deformation occurs. Variations in the airflow velocity can therefore be determined by measuring the changes in resistance caused by the beam deflection using an inductance-capacitance-resistance (LCR) meter. The experimental data indicate that the proposed gas flow sensor has a high sensitivity ( $0.0533 \Omega/\text{ms}^{-1}$ ), a high measurement limit ( $45 \text{ ms}^{-1}$ ) and a short response time (1.38 s).

---

\*Corresponding author, e-mail address: cylee333@ms74.hinet.net

## 1. Introduction

In the last decade, emerging micro-electro-mechanical system (MEMS) and micromachining techniques have led to the development of miniaturized sensing instrumentation capable of accessing information at a microscale level. Importantly, the functionality and reliability of these microsensors can be increased through their integration with mature logic IC technology or with other sensors.

Flow measurement is an essential task in such diverse fields as medical instrumentation, process control, and environmental monitoring. Many previous studies have addressed the development and application of MEMS techniques to the fabrication of flowmeters. A review of the related literature reveals that flowmeters can be broadly categorized as either thermal or nonthermal in their sensing approach. Flowmeters incorporating a microcantilever loaded on one side with a piezoresistive material have attracted particular interest. Such meters typically provide high-sensitivity, high-linearity and high-stability measurement characteristics. When airflow passes over the cantilever beam, a deformation occurs and this induces a variation in the resistance of the piezoresistor layer deposited on the beam. The flow rate can then be determined by measuring the change in resistance. These devices are attractive since they provide high-precision flow measurement results and are physically very small and hence highly portable. In this study, we develop a novel fabrication process for microcantilever-based flow sensors featuring suspended nitride/silicon microcantilevers.

MEMS technology has facilitated the development of a particular class of thermal gas flowmeters that use resistors as a sensing element to carry out thermal evaluation.<sup>(1-5)</sup> In these sensors, the temperature difference between the sensing resistors varies as the gas flow rate changes, and the change in resistance enables the gas flow rate to be precisely determined. Qiu et al. presented a micro-gas-flow-sensor integrated with a heat sink and a flow guide on the underside of the sensing element.<sup>(1)</sup> This device was capable of measuring flow velocities of up to  $5 \text{ ms}^{-1}$  and had a power consumption of 8 mW. Neda et al. fabricated a single-wire thermal flowmeter featuring a polysilicon microheater.<sup>(2)</sup> The sensor provided a wide flow measurement range of  $0.005\text{--}35 \text{ ms}^{-1}$  and demonstrated a rapid response time of just 0.14 ms (90%) with a power consumption of 6 mW. Maily et al. developed a flowmeter using a hot platinum thin film ( $3000 \text{ \AA}$ ) deposited on a  $\text{SiN}_x$  membrane ( $5000 \text{ \AA}$ ).<sup>(4)</sup> The response time and measurement range of the meter were 6 ms and  $0\text{--}20 \text{ ms}^{-1}$ , respectively, with a power consumption of 20 mW. In a later study, Kim et al. presented a micromachined circular thermal flow sensor capable of detecting both the flow direction and the velocity simultaneously.<sup>(5)</sup> However, the power consumption of this device exceeded 80 mW. More recently, nonthermal gas flowmeters have been developed. These devices typically have the advantages of lower power consumption and an improved potential for integration with other sensors. Svedin et al. fabricated a static turbine flowmeter with a micromachined silicon torque sensor.<sup>(6)</sup> Although this design did not require microheaters and had low power consumption, the assembly was elaborate and hence the fabrication costs were high. Su et al. developed a piezoresistive flowmeter with a silicon cantilever probe. In their approach, the gas flow was measured by a strain gauge

attached to the root of the cantilever beam. The measurement range was shown to be 0.07–20  $\text{ms}^{-1}$ .<sup>(7)</sup> However, the proposed device was unable to measure higher flow rates, i.e., 40  $\text{ms}^{-1}$ , for increasing its practicability.

Lee and Lee developed a simple and reliable fabrication method for microcantilevers designed for humidity sensing applications.<sup>(8)</sup> In the current study, we develop a novel process for the fabrication of a Pt-based gas flow sensor incorporating a microcantilever structure. The current approach utilizes the bending-up effect of the cantilever caused by residual stress induced during the steps in the fabrication process. The bending-up structure not only increases the sensitivity of the flow sensor, but also is reliable at higher flow rates due to its measurement of air flow in the downstream direction. The proposed sensor is easily fabricated and provides an extended measurement range. The experimental data reveal that the sensor has a high sensitivity ( $0.0533 \Omega/\text{ms}^{-1}$ ), a high measurement limit ( $45 \text{ ms}^{-1}$ ) and a short response time (1.38 s).

## 2. Design

### 2.1 Cantilever deflection induced by thermal stress

Figure 1 shows a schematic illustration of the current bimorph microcantilever and the corresponding geometrical model. In this study, a thin film of silicon nitride is deposited on a silicon beam. In the model shown in Fig. 1, the thicknesses of the film and beam are denoted as  $t_1$  and  $t_2$ , respectively. (Note that hereafter, subscripts 1 and 2 are used to indicate the film and beam, respectively). The mismatch between the thermal expansion coefficients of the film and beam which arises when the microcantilever is subjected to thermal loading induces different thermal deformations of the two components and this causes residual stresses to be generated within the structure. Figure 2 shows a schematic

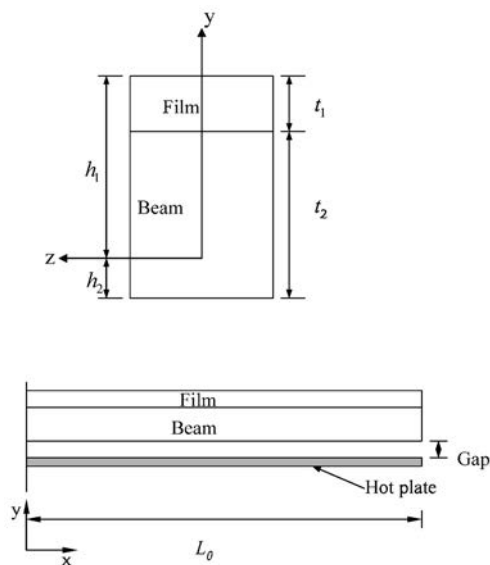


Fig. 1. Geometrical model of bimorph microcantilever.<sup>(9)</sup>

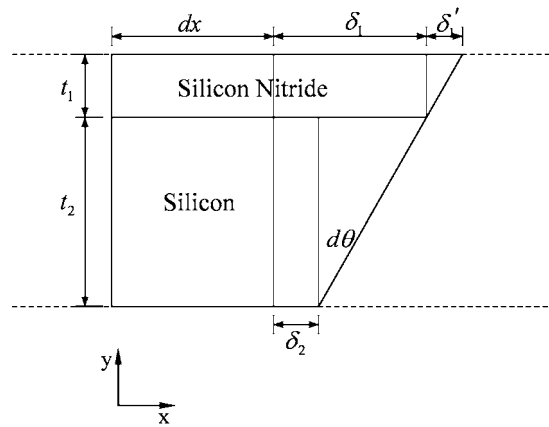


Fig. 2. Schematic diagram of deformed microcantilever.<sup>(9)</sup>

diagram of the deformed microcantilever. The relationship between the microcantilever displacement and the film and beam thicknesses is given approximately by

$$(t_1 + t_2)d\theta = \delta_1 + \delta_1' - \delta_2, \quad (1)$$

where  $\delta_1$  and  $\delta_2$  are the displacements of the film and beam caused by thermal expansion. From the geometrical similarity in Fig. 2, it can be shown that the relationship among  $\delta_1$ ,  $\delta_2$ ,  $t_1$ , and  $t_2$  is given by

$$\frac{\delta_1 - \delta_2}{t_2} = \frac{\delta_1'}{t_1}. \quad (2)$$

Substituting eq. (2) and the relationships  $\delta_1 = \alpha_1 \Delta T dx$  and  $\delta_2 = \alpha_2 \Delta T dx$  into eq. (1) yields

$$(t_1 + t_2)d\theta = \Delta T(\alpha_1 - \alpha_2) \left(1 + \frac{t_1}{t_2}\right) dx, \quad (3)$$

where  $\Delta T$  is the temperature rise and  $\alpha_1$  and  $\alpha_2$  are the coefficients of thermal expansion of the film and beam, respectively. The coefficients of thermal expansion of the electrode, film and beam are shown in Table 1. Equation (3) can be rewritten as

$$\frac{d\theta}{dx} = \frac{\Delta T(\alpha_1 - \alpha_2) \left(1 + \frac{t_1}{t_2}\right)}{t_1 + t_2}. \quad (4)$$

Table 1  
Coefficients of thermal expansion of materials applied in present study.

Material	Coefficient of thermal expansion ( $^{\circ}\text{C}^{-1}$ )
Platinum	$9.1 \times 10^{-6}$
Silicon	$4.05 \times 10^{-6}$
Silicon nitride	$3.0 \times 10^{-5}$

The equations of the microcantilever slope  $\theta$  and deflection  $v$  can be obtained by integrating eq. (4) once and twice, respectively, i.e.,

$$\theta = \frac{\Delta T(\alpha_1 - \alpha_2) \left(1 + \frac{t_1}{t_2}\right)}{t_1 + t_2} x + C_1 \quad (5)$$

$$v = \frac{\Delta T(\alpha_1 - \alpha_2) \left(1 + \frac{t_1}{t_2}\right)}{t_1 + t_2} \frac{x^2}{2} + C_1 x + C_2, \quad (6)$$

where  $C_1$  and  $C_2$  are integration constants and are evaluated from known conditions pertaining to the slope and deflection, respectively. Obviously, the slope and deflection at the fixed support end of the cantilever are zero. Under these boundary conditions, the constants  $C_1$  and  $C_2$  must therefore also be equal to zero. The deflection at the free end of the beam,  $\delta$ , can then be calculated from

$$\delta = \frac{\Delta T(\alpha_1 - \alpha_2) \left(1 + \frac{t_1}{t_2}\right) L^2}{2(t_1 + t_2)}, \quad (7)$$

where  $L$  is the length of the microcantilever.<sup>(9)</sup>

## 2.2 Sensing principle

In the developed flow sensor, the deformation of the microcantilever beam under different airflow velocities is established by platinum resistance measurement procedure, as indicated in Fig. 3. Note that Au is used as the bonding pads to connect the external LCR meter since the resistivity of Au is less than that of Pt and therefore the resistance effect of the leads is reduced. The resistance measurement is based on the formula

$$R = \frac{l\rho}{A}, \quad (8)$$

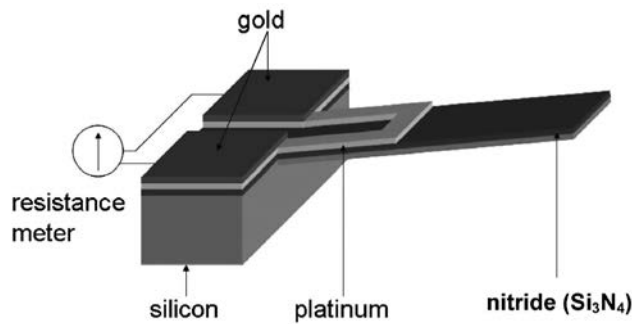


Fig. 3. Schematic illustration of gas flow sensor.

where  $R$  is the resistance,  $l$  is the resistor length,  $\rho$  is the resistivity, and  $A$  is the cross-sectional area of the resistor. From eq. (8), it is clear that the dimensions of the resistor have a direct effect on the measured resistance. In the current study, a resistor layer is deposited on the cantilever structure. When airflow passes over the cantilever beam, a deformation of the resistor occurs, as shown in Fig. 4. Variations in the airflow velocity are then determined by measuring the corresponding change in the resistance using the LCR meter.

### 2.3 Shape design

Figure 5 shows the dimensions of the cantilever beam and platinum resistors considered in this study. In these figures, the black netted area corresponds to the platinum resistor, whereas the periphery of the black line indicates the cantilever beam. As shown, platinum resistors with four different dimensions are fabricated on microcantilevers of the same size to investigate the relationship between the resistor dimensions and the sensitivity of the gas flow sensor. The resonant frequency of the cantilever is calculated to be 1.94 KHz.

## 3. Fabrication

Figure 6 shows an overview of the fabrication process used for the current micromachined gas flow sensors. Initially, a low-stress nitride layer of thickness  $1.0\ \mu\text{m}$  was deposited on either side of a  $500\text{-}\mu\text{m}$ -thick double-side-polished silicon wafer. A thin layer of Cr ( $0.02\ \mu\text{m}$ ) was then deposited on the upper surface of the wafer to form an adhesion layer for the subsequent deposition of the platinum resistors. The platinum resistors ( $0.1\ \mu\text{m}$  thickness) were deposited using an electron-beam evaporation process. The same technique was then used to deposit a layer of Au ( $0.4\ \mu\text{m}$  thickness) on the resistors to serve as an electrode and to provide electrical leads.

To form the microcantilever beam, the cantilever structure and a back-etching nitride mask were patterned in  $\text{SF}_6$  RIE plasma. In the etching process, a paddle structure was released in a KOH etchant (40 wt%,  $85^\circ\text{C}$ , supplied by J. T. Baker). After etching, the total microcantilever beam thickness was  $20\ \mu\text{m}$  (nitride:  $1\ \mu\text{m}$  / silicon:  $19\ \mu\text{m}$ ) and the cantilever paddle exhibited an upward bending effect as a result of the stress relaxation caused by the thermal stress induced in the heating and cooling steps performed before

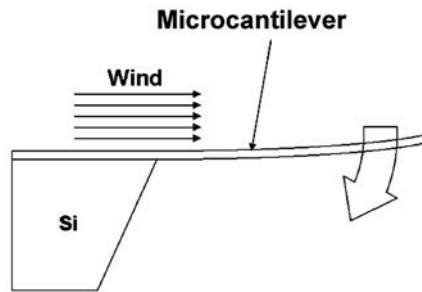


Fig. 4. Diagram of gas flow sensor during sensing operation.

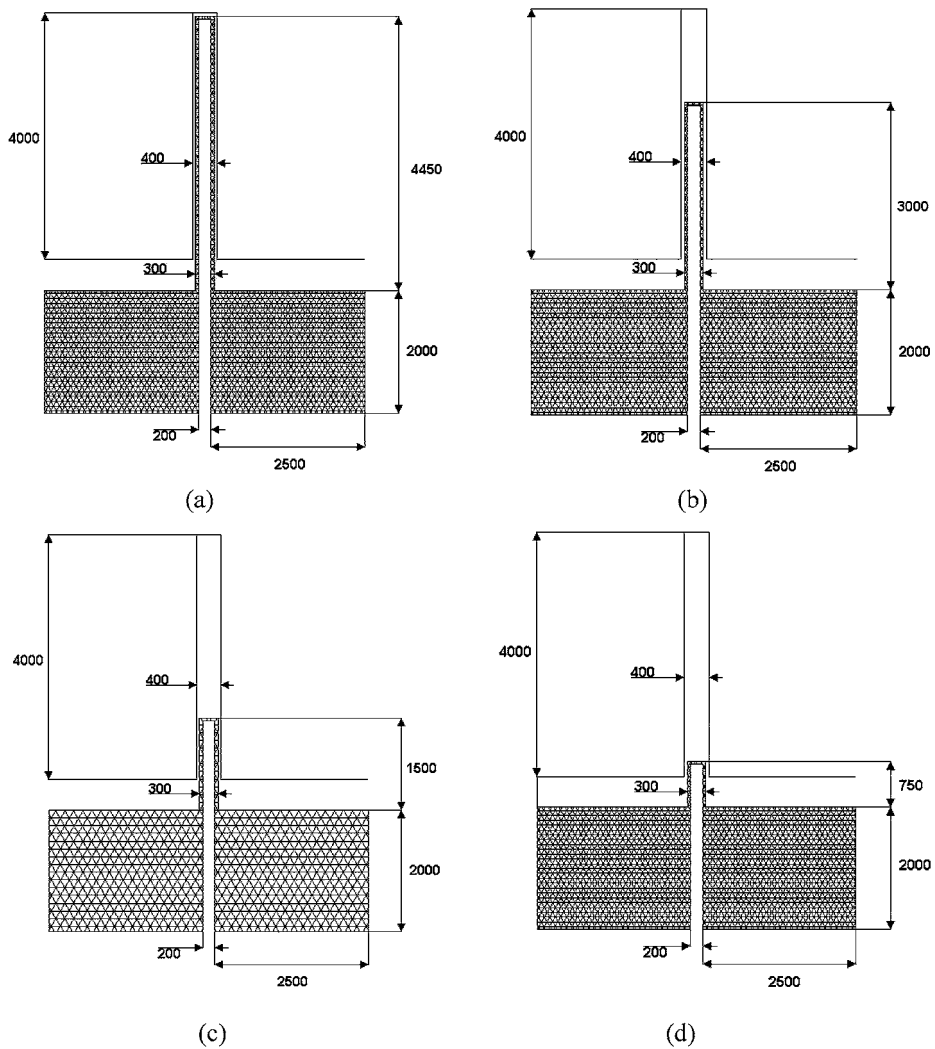


Fig. 5. Dimensions of cantilever beams with different Pt resistor lengths. (a)  $l = 4450 \mu\text{m}$ , (b)  $l = 3000 \mu\text{m}$ , (c)  $l = 1500 \mu\text{m}$  and (d)  $l = 750 \mu\text{m}$ .

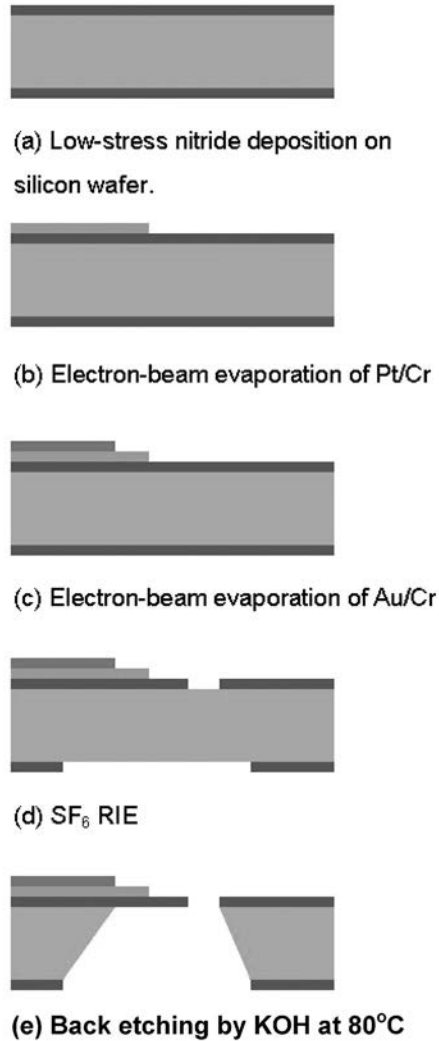


Fig. 6. Overview of fabrication process employed for proposed gas flow sensor.

etching and the stress induced in the deposition step of the nitride layer. This phenomenon causes an initial beam deformation position that assists the flow rate sensing function. To increase the reliability of the microcantilever, a small thickness of silicon was retained to act as an understructure. Figure 7 shows a scanning electron microscopy (SEM) image of a typical freestanding structure fabricated in this study.

#### 4. Results and Discussion

A systematic investigation was conducted into the performance of the fabricated micro-gas-flow-sensors. The characterization of the sensors was carried out in a wind tunnel



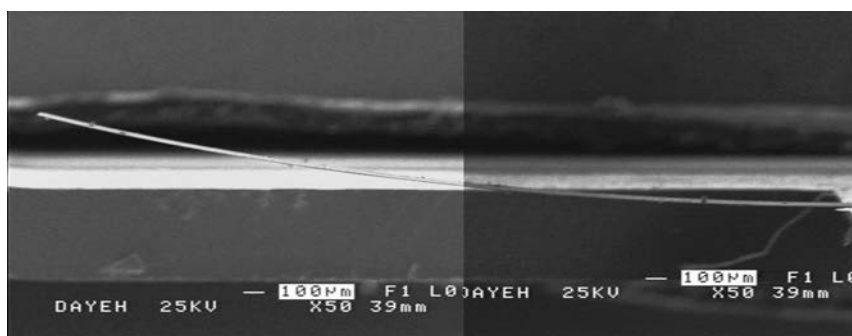


Fig. 7. Side-view SEM image of cantilever beam.

using different airflow velocities. The variation in the sensor resistance as the airflow passed over the cantilever was measured using an LCR meter (4263B, Agilent Technologies), which was connected to the flow sensors to record the signal response. The LCR meter had a working frequency in the range of 100 Hz–100 KHz and 1.5 to 2  $V_{dc}$  bias voltage. For reference purposes, a Pitot tube flowmeter was also used to measure the velocity of the airflow.

#### 4.1 Sensitivity of gas flow sensors

As shown in Fig. 8, the resistance of the current micro-gas-flow-sensors increases linearly with the airflow rate. As shown in Table 2, for a constant temperature of 30°C, the average sensitivity values are found to be 0.0014, 0.0145, 0.0282, and 0.0533 ( $\Omega/\text{ms}^{-1}$ ) for platinum resistors with lengths of ( $l$ ) 750  $\mu\text{m}$ , 1500  $\mu\text{m}$ , 3000  $\mu\text{m}$ , and 4450  $\mu\text{m}$ , respectively, with a maximum error of 2%. Therefore, it is clear that the flow rate sensitivity increases with increasing resistor length. The maximum detectable flow rate is found to be 45  $\text{ms}^{-1}$ , which is approximately twice that of the gas flowmeter incorporating a silicon cantilever presented in ref. 7.

#### 4.2 Thermal effect on flow sensors

Figure 9 shows the relationship between the sensitivity performance and temperature for the flow sensor with platinum resistors with a length of 4450  $\mu\text{m}$ . The sensitivity of the sensors increases when temperature increases. The average sensitivities are found to be 0.0503, 0.0533, and 0.0556 ( $\Omega/\text{ms}^{-1}$ ) for three temperatures (20, 30, and 40°C, respectively).

#### 4.3 Stability of gas flow sensors

The experimental results indicate that at a constant flow rate of 30  $\text{ms}^{-1}$  and a temperature of 30°C, the variation in stability of the four gas flow sensors is small, i.e., 0.00027% F.S., 0.000123% F.S., 0.000162% F.S., and 0.000178% F.S. for resistor lengths ( $l$ ) of 750  $\mu\text{m}$ , 1500  $\mu\text{m}$ , 3000  $\mu\text{m}$ , and 4450  $\mu\text{m}$ , respectively (Fig. 10). The total time of measurement period was 70 s.

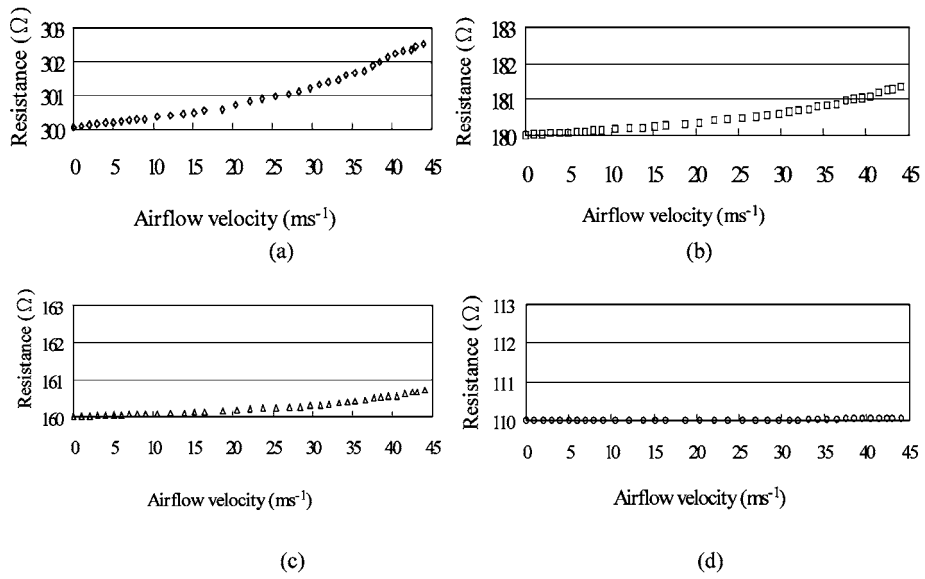


Fig. 8. Experimental comparisons of flow rate sensitivity for sensors with Pt resistor lengths of (a)  $l = 4450 \mu\text{m}$  [ $\diamond$ ], (b)  $l = 3000 \mu\text{m}$  [ $\square$ ], (c)  $l = 1500 \mu\text{m}$  [ $\Delta$ ], and (d)  $l = 750 \mu\text{m}$  [ $\circ$ ].

Table 2  
Sensitivity of gas flow sensors with different electrode lengths.

Dimension $l$ ( $\mu\text{m}$ )	Sensitivity ( $\Omega/\text{ms}^{-1}$ )
4450	0.0533
3000	0.0282
1500	0.0145
750	0.0014

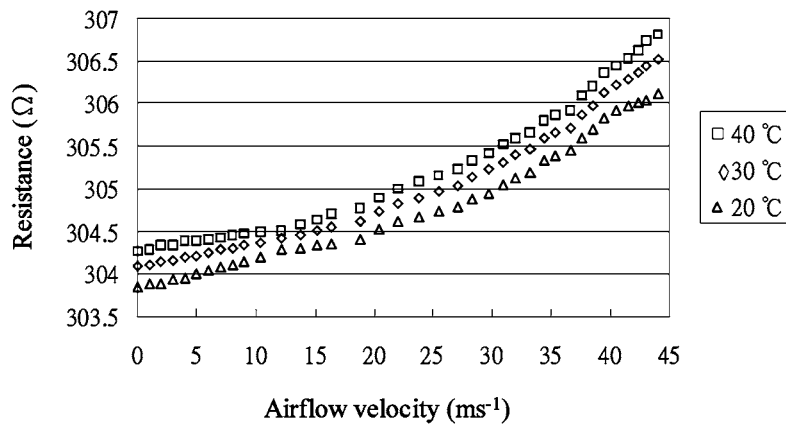


Fig. 9. Temperature effect of flow rate sensitivity for three temperatures (20, 30, and 40°C).

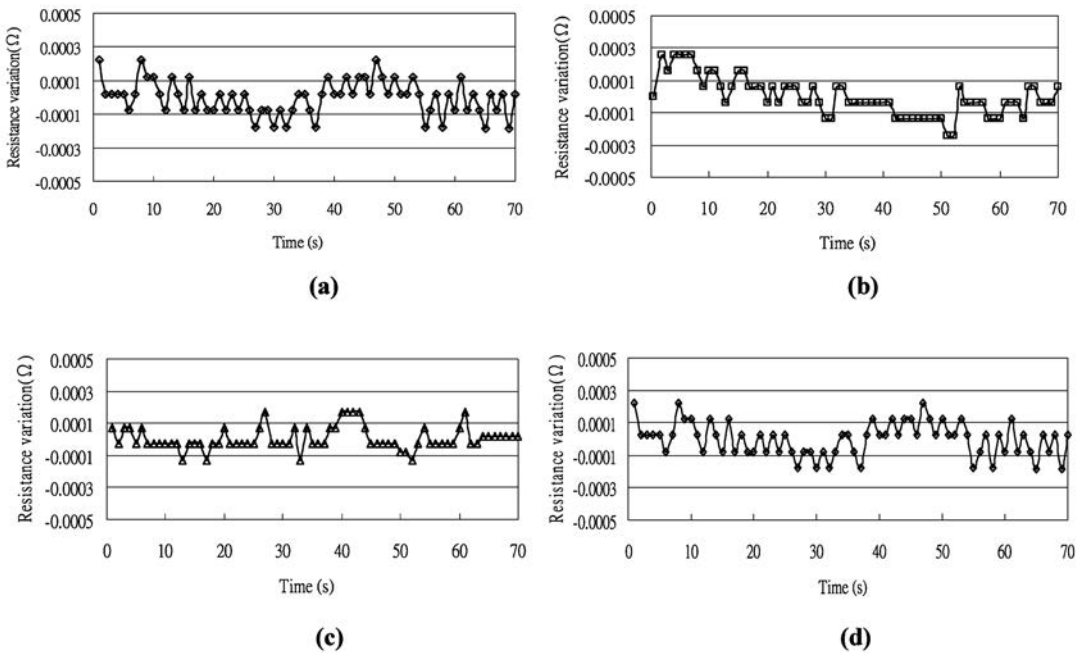


Fig. 10. Stability with Pt resistor lengths of (a)  $l = 4450 \mu\text{m}$  [◇], (b)  $l = 3000 \mu\text{m}$  [□], (c)  $l = 1500 \mu\text{m}$  [Δ], and (d)  $l = 750 \mu\text{m}$  [○].

#### 4.4 Time response of gas flow sensors

The time response of piezoresistive gas flowmeters is not addressed in previous related studies. However, it is known that the response time of thermal flow meters varies from 0.14 ms to 150 ms. It is also essential to investigate this performance in nonthermal gas flowmeters. Figure 11 shows the time response obtained for the current flow sensor with a resistor length of 4450  $\mu\text{m}$ . The average time constant of the microcantilever-based gas flow sensor is found to be 1.38 s (90%) for gas flow rates in the range of 0 to 30  $\text{ms}^{-1}$ .

#### 4.5 Sensing hysteresis of gas flow sensors

Previous studies have not addressed the sensing hysteresis of gas flowmeters. Ideally, a sensor should follow the same resistance path as the gas flow rate is increased or decreased. However, in practice, most sensors exhibit a small degree of hysteresis. Figure 12 shows the sensing hysteresis of the proposed resistive gas flow sensor ( $l = 3000 \mu\text{m}$ ). In this investigation, the temperature was maintained constant at 30°C while the gas flow rate was progressively increased from 0  $\text{ms}^{-1}$  to 45  $\text{ms}^{-1}$  over a period of 30 min and then reduced to 0  $\text{ms}^{-1}$  at the same rate. The results show that the resistive gas flowmeter has a hysteresis of 25% F.S., which implies that sensing hysteresis is an important consideration in the design of cantilever-based sensors.

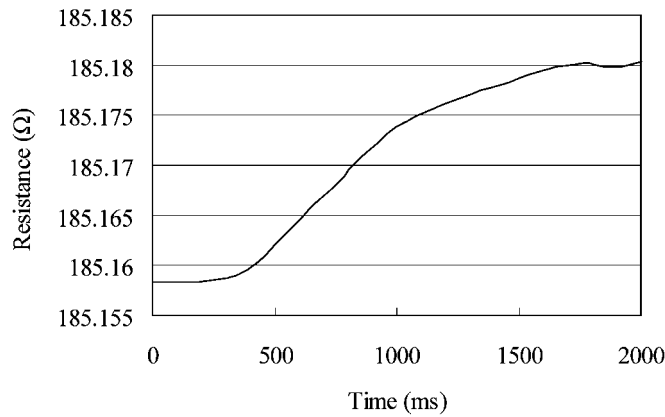


Fig. 11 Time response of gas flow sensor for gas flow rate range of 0  $\text{ms}^{-1}$  to 30  $\text{ms}^{-1}$ .

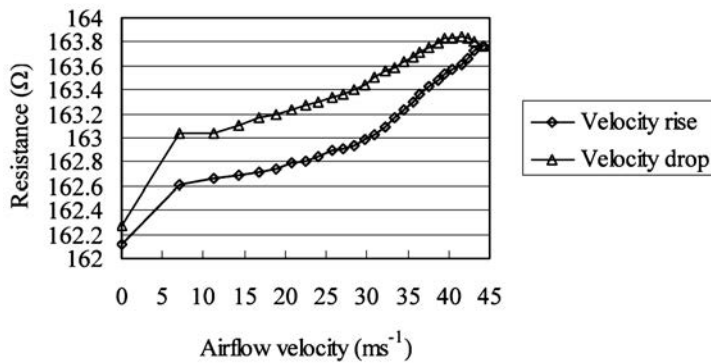


Fig. 12 Sensing hysteresis of gas flow sensor.

## 5. Conclusions

In this study, we have successfully demonstrated a novel micromachined silicon cantilever paddle for high-flow-rate sensing. A new fabrication process has been developed for the manufacture of silicon microstructures integrated with a Pt resistor. It has been shown that the deflection of a freestanding silicon member caused by a gas flow passing over the cantilever paddle gives rise to a measurable change in the resistance of the Pt resistor. The proposed gas flow sensor demonstrates a sensitivity of  $0.0533 \text{ } \Omega/\text{ms}^{-1}$  and a maximum measurable flow rate of  $45 \text{ ms}^{-1}$ . In addition to its high gas flow rate sensitivity and wide flow rate range, the device also exhibits a high degree of stability and a rapid time response. However, a hysteresis of 25% F.S. is observed.

Flowmeters are widely applied in diverse fields. Therefore, a strong demand exists for simply fabricated gas flowmeters in many fields. The cantilever-based sensor presented in this study is well suited to meet this demand.

### **Acknowledgements**

The authors would like to acknowledge the financial support provided by the National Science Council in Taiwan (NSC 95-2211-E-212-058 and NSC 95-2218-E-006-022).

### **References**

- 1 L. Qiu, S. Hein, E. Obermeier and A. Schubert: *Sens. Actuators, A* **54** (1996) 547.
- 2 T. Neda, K. Nakmura and T. Takumi: *Sens. Actuators, A* **54** (1996) 626.
- 3 K. A. A. Makinwa and J. H. Huijsing: *Sens. Actuators, A* **92** (2001) 280.
- 4 F. Mailly, A. Giani, R. Bonnot, P. Temple-Boyer, F. Pascal-Delannoy, A. Foucaran and A. Boyer: *Sens. Actuators, A* **94** (2001) 32.
- 5 S. Kim, T. Nam and S. Park: *Sens. Actuators, A* **114** (2004) 312.
- 6 N. Svedin, E. Stemme and G. Stemme: *J. Micro-Electro-Mechanical Systems* **12**(6) (2003) 937.
- 7 Y. Su, A. G. R. Evans, A. Brunnschweiler and G. Ensell: *J. Micromech. Microeng.* **12** (2002) 780.
- 8 C. Y. Lee and G. B. Lee: *J. Micromech. Microeng.* **13** (2003) 620.
- 9 C. Y. Lee, C. H. Tsai, L. W. Chen, L. M. Fu and Y. C. Chen: *J. Microsystem Technologies* **12** (2006) 979.